Journal of Catalysis **193,** 283–294 (2000)
doi:10.1006/jcat.2000.2898, available online at http://www.idealibrary.com on IDEAL®

Combined Alkyl and Sulfonic Acid Functionalization of MCM-41-Type Silica

Part 1. Synthesis and Characterization

Isabel Díaz, Carlos Márquez-Alvarez, Federico Mohino, Joaquín Pérez-Pariente,[1] and Enrique Sastre

Instituto de Catálisis y Petroleoquímica (CSIC), Campus Cantoblanco, 28049 Madrid, Spain

Received January 5, 2000; revised March 30, 2000; accepted April 10, 2000

Single-step synthesis of well-ordered MCM-41 materials containing simultaneously alkyl (methyl or propyl) and 3-mercaptopropyl groups has been carried out by hydrothermal treatment of gels containing a mixture of dodecyl and hexadecyltrimethylammonium surfactants. A wide range of synthesis conditions has been studied in order to optimize the pore arrangement and to vary the alkyl/mercaptopropyl ratio of the product. A number of characterization techniques suggest that the anchored organic fragments lined the wall channels of the MCM-41 in a close-packed configuration. The mercaptopropyl groups can be oxidized with hydrogen peroxide to sulfonic acid with a high retention of sulfur and no loss of methyl groups.

Key Words: **MCM-41; mesoporous acid catalysts; sulfonic acid; fatty acids; selective esterification; monoglyceride.**

INTRODUCTION

The fatty acid monoesters of glycerol are valuable chemical products widely used as emulsifiers in the food, pharmaceutical, and cosmetics industries (1, 2). There are two main preparative routes to obtain monoglycerides: the transesterification of the triglycerides with glycerol at high temperature in the presence of a basic catalyst, and the direct esterification of glycerol with fatty acids (3, 4). Investigations to optimize the yield of the monoderivative in both processes are of great interest. Benefits and drawbacks of glycerolysis have been outlined in Ref. (4). High temperature, in the range of 493–523 K, and glycerol/triglyceride ratios above the stoichiometry are usually required. A recent example of glycerolysis catalyzed by alkaline oxides is given in Ref. (3). Although the catalysts described in this work exhibit good activity, a glycerol/oil molar ratio of 12 is required to obtain a high yield of monoglyceride.

The direct esterification of the polyol with a fatty acid is catalyzed by strong mineral or organic acids, like sulfonic acid (5). In the strategy for developing highly selective catalysts towards the monoderivative, zeolites have been tested as potential suitable materials, owing to their well-known acid strength and size limitation imposed to the reaction products by the pore dimension. Although acid zeolites are, in general, good esterification catalysts for relatively small substrates (6), their performance in glycerol esterification with fatty acids (hydrocarbon chain higher than C_{10}) is below expectations. Large-pore 12-MR zeolites have been used as catalysts, but in this case modest yields of monoglyceride were obtained from lauric acid (7, 8) and oleic acid (9, 10).

Very recently, MCM-41-type mesoporous silicas functionalized with sulfonic acid groups have been reported to selectively catalyze this reaction (11). These materials can be prepared either by silylation of pure silica or by co-condensation of alkoxysilanes and 3-mercaptopropyltrimethoxysilane (12–15) which is further oxidized to obtain propylsulfonic acid groups anchored onto framework silicon atoms. These [SO_3H]–MCM-41 mesoporous catalysts combine a high acidity and a good accessibility to the active centers, owing to the presence of channels with large diameter, higher than 1.4 nm.

Besides the pore size and the strength of the active acid sites, the relative affinity of the catalyst for the highly hydrophilic glycerol and the rather hydrophobic fatty acid also influence the catalytic activity. Moreover, an efficient removal from the catalyst surface of the water formed during the reaction would benefit the overall conversion. It has been reported that the activity of USY catalysts in the esterification of benzoic and phenylacetic acids with short-chain alcohols increases with the hydrophobicity of the catalyst (6). Also, the higher activity and selectivity of [SO_3H]–MCM materials in the reaction of sorbitol with lauric acid in comparison with zeolites have been attributed to the higher hydrophobicity of the former (14, 16).

Therefore, it would be desirable to tune the hydrophobic/hydrophilic balance of the catalyst to that required by

[1] To whom correspondence should be addressed. Fax: +34-91 585 47 60. E-mail: jperez@icp.csic.es.

0021-9517/00 $35.00

the specific esterification reaction, in order to improve both activity and selectivity. It has been recently reported that hybrid mesoporous materials bearing organic groups prepared by copolymerization are more hydrophobic than the organic-free counterparts (17). The benefits of tuning the catalyst hydrophobicity where substrates of very different polarity are involved have already been reported in the case of olefin epoxidation with hydrogen peroxide and *tert*-butylhydroperoxide catalyzed by Ti–MCM-41 (18, 19).

In this paper, we report a new synthesis strategy in order to obtain well-ordered, hybrid MCM-41 materials bearing both alkyl and sulfonic groups. First, the synthesis and characterization of those materials having different contents of sulfonic and alkyl groups and pore sizes will be described. In a second paper (20), the influence of the catalysts textural properties and surface groups on their performance in the esterification of glycerol with lauric and oleic acids will be presented.

METHODS

(a) Synthesis Procedure

Combined alkyl- and mercaptopropyl-functionalized MCM-41-type silica materials, [R/SH]–MCM-41, have been prepared by co-condensation of tetramethylorthosilicate (TMOS, Aldrich) and 3-mercaptopropyltrimethoxysilane (MPTS, Sigma), with either methyl- (MTMS, Aldrich) or propyl- (PTMS, Aldrich) trimethoxysilane. Prior to this work, we have observed that the use of a mixture of surfactants with different chain lengths, the simultaneous replacement of the NaOH commonly used in the reported synthesis of thiol–MCM-41 by tetramethylammonium hydroxide (TMAOH), and the evaporation of the methanol prior to gel autoclaving strongly improved the ordering of the functionalized MCM-41 materials (21, 22). Therefore, we have used the same synthesis approach in this work. According to this procedure, synthesis gels of the general molar composition $[1-(x+y)]$ TMOS : x MPTS : y (MTMS or PTMS) : u (C_{16}TAB or C_{12}TAB) : v (C_{12}TAB or C_{10}TAB) : 0.27 TMAOH : 18.8 MeOH : 77.7 H_2O were prepared, where C_{16}TAB, C_{12}TAB, and C_{10}TAB stand for hexadecyltrimethylammonium (Aldrich), dodecyltrimethylammonium (Fluka), and decyltrimethylammonium (Fluka) bromides, respectively. In general, C_{16}TAB and C_{12}TAB were used as surfactants, and only in two preparations was a mixture of C_{12}TAB and C_{10}TAB used. Attempts to increase the pore size by addition of trimethylbenzene (TMB) were also made.

The chemical compositions for several synthesis gels are given in Table 1. In a typical synthesis procedure, 1.74 g of C_{16}TAB and 0.61 g of C_{12}TAB were dissolved in a mixture of 33.78 g of methanol and 74.16 g of deionized water, in a 250-ml beaker made of polypropylene. A mixture of 6.18 g of TMOS, 2.87 g of MPTS, and 0.23 g of MTMS was added to this solution. Finally, 5.52 g of TMAOH solution (25 wt% in water, Aldrich) was also added to the resulting mixture. The obtained gel was stirred at 293 K for 16 h to evaporate all the methanol, and then the reaction mixture was introduced into 60-ml Teflon-lined stainless steel autoclaves which were heated at 368 K for 48 h without stirring. The solid products were recovered by filtration, washed, and dried at 333 K. When TMB was required it was added to the solution of surfactants in methanol/water (TMB/surfactant mol ratio = 0.5–1). The surfactant was removed by stirring 1.5 g of the dried sample with a solution of 20 ml of HCl (35 wt%) in 205 ml of ethanol at 343 K for 24 h. The quantitative removal of the surfactant (N content lower than 0.1 wt%) required in general two consecutive extractions. The oxidation of the mercaptopropyl group to sulfonic acid was carried out by treating 1 g of the extracted sample with 16 ml of H_2O_2 (33 vol%), followed by washing, acidification with 0.05 M sulfuric acid, washing again, and drying of the solid at 333 K.

TABLE 1

Textural Properties Determined after Surfactant Extraction for the Samples Prepared with the Following Gel Composition: 0.71 TMOS : x MPTS : y RTMS : 0.085 C_{16}TAB : 0.035 C_{12}TAB : 0.27 TMAOH : 18.8 MeOH : 77.7 H_2O[a]

Sample	x	y	BET surface area/$m^2\,g^{-1}$	Unit cell parameter (XRD)/Å	Pore diameter (BJH)/Å	Mesopore volume/$cm^3\,g^{-1}$
M0	0.290	0	579	39	12	0.29
M5	0.275	0.015	719	38	13	0.34
M10	0.261	0.029	800	40	13	0.29
M40	0.174	0.116	853	40	13	0.27
M60	0.116	0.174	850	40	14	0.29
Mp10	0.261	0.029	843	39	13	0.29
Ms10[b]	0.261	0.029	744	33	<10	0.18

[a] RTMS stands for MTMS in all samples except for Mp10, for which PTMS was used instead. See text for chemicals' short name codes.

[b] Sample synthesized using C_{12}TAB and C_{10}TAB as surfactants, in the ratio 0.085 and 0.035 molecules of surfactant per Si atom in the gel, respectively.

(b) Characterization

Analysis of the organic material present in the solid was carried out using a Perkin-Elmer 2400 CHN analyzer. The concentration of surface sulfonic acid groups in the oxidized samples was determined by titration. Thermogravimetric analysis (TGA) was performed using a Perkin-Elmer TGA7 instrument, from 303 to 1173 K at a heating rate of 10 K min^{-1} under air flow. TG/MS analyses were performed using a Perkin-Elmer TGA7 thermobalance coupled to a Fisons MD-800 mass spectrometer through a Perkin-Elmer interface. Samples were heated under a He flow (ca. 100 ml min^{-1}) from 303 to 1173 K at a heating

rate of 20 K min^{-1} and the outlet gases were analyzed in the mass spectrometer with a frequency of 30 scans/min (2 to 350 amu). The spectrometer was operated at 70 eV. X-ray powder diffraction patterns were collected using a Seifert XRD 3000P diffractometer operating at low angle (2θ from 1 to 10°). Cu$K\alpha$ radiation was applied using 1- and 0.5-mm font gratings and a 0.1-mm detector grating. Micrographs and electron diffraction patterns were recorded using a JEOL FX 200 transmission electron microscope operating at 200 kV. Adsorption of nitrogen was carried out at 77 K using a Micromeritics ASAP 2000 apparatus. Specific surface areas were calculated following the BET procedure. Pore size distribution was obtained by using the BJH pore analysis applied to the desorption branch of the nitrogen adsorption/desorption isotherm. Infrared spectra of the solid samples diluted in KBr were recorded at room temperature in the transmission mode, in the range 4000 to 400 cm^{-1} at 4 cm^{-1} resolution, using a Nicolet 5ZDX FTIR spectrometer provided with a TCD detector. For calibration purposes spectra of methyltrimethoxysilane (MTMS, Aldrich) solutions in 2-butanol (99.5%, Aldrich) were also recorded using an 80-μm-path length Perkin-Elmer liquid cell provided with flat KBr windows. ^{13}C CP MAS NMR spectra were recorded using a Varian VXR S-400 WB instrument. The ^{1}H–^{13}C contact time was 4 ms and the recycle delay 3 s. X-ray photoelectron spectra (XPS) were obtained using a Fisons Escalab 200R spectrometer provided with a hemispherical electron analyzer and an Mg anode X-ray exciting source (Mg$K\alpha$ energy = 1253.6 eV). Binding energies (±0.2 eV) were corrected for charge effects by referencing to the O 1*s* peak at 532.9 eV.

RESULTS

(a) Synthesis of [R/SH]–MCM-41 Materials

Several ratios of organic siloxanes (both propylthiol and methyl or propyl functional groups) to tetramethylorthosilicate in the synthesis mixture have been tested, aiming to obtain well-ordered materials with a content of functional groups as high as possible. In order to meet both requirements, the fraction of functionalized silicon atoms in the synthesis gel ($x+y$) was set to 0.29 (Table 1), based on a preliminary study. Two syntheses were carried out with gels having an organic content ($x+y$) as high as 0.65 and 0.45, that rendered amorphous solids. Decreasing the silane ratio to 0.36 led to a material that showed a broad low-angle reflection in the X-ray pattern. A further reduction of the total silane content to 0.29 resulted in materials that showed several XRD reflections, evidencing a highly ordered structure.

The X-ray diffraction (XRD) patterns of as-made, extracted, and oxidized [R/SH]–MCM-41 materials are similar for all those samples obtained from gels with an alkyl : thiol ratio ranging from 1/9 to 2/3. The pattern of the as-made samples (Fig. 1) show an intense peak corresponding to the d_{100} reflection, which is accompanied by weaker reflections at 2θ close to 4.4° and 5.1°, corresponding to the d_{110} and d_{200} spacing of the hexagonal symmetry *p*6*mm* of MCM-41, respectively. This indicates that only one MCM-41 phase is obtained, despite the use of a mixture of C_{16} and C_{12} surfactants. For the sample M0, which does not contain organic groups other than propylthiol, only the intense and broader d_{100} reflection is distinguished (22). Therefore, the incorporation of alkyl groups to the thiol–MCM-41 materials seems to improve the ordering of the pore rearrangement, and this effect is more clearly evidenced after removal of the surfactant by the HCl/EtOH treatment.

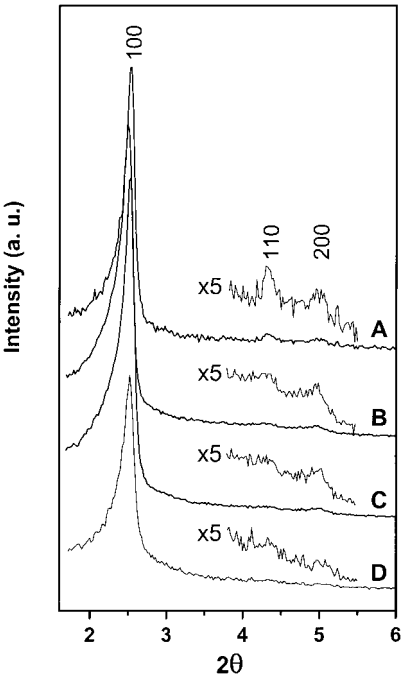

FIG. 1. XRD patterns of the M60 sample as-made (A), extracted (B), and oxidized (C) and the extracted sample M0e (D).

The unit cell parameter ($a_0 = 2d_{100}/\sqrt{3}$) of these materials is close to 40 Å, and remains practically unaffected by partial replacement of the mercaptopropyl by alkyl groups in the synthesis gel (Table 1).

The TEM images and selected area electron diffraction (ED) patterns of a representative sample with high Me content (M40) evidence the well-ordered hexagonal array of pores (Fig. 2). From those ED patterns, a unit cell value of 3.9 nm is obtained, in excellent agreement with that derived from XRD (Table 1). EDS analysis in the TEM chamber indicated that in all the alkyl/propylthiol samples, the sulfur is homogeneously distributed through the solid. Its concentration measured by this technique is within ±15% of that determined by bulk analysis.

The organic content of the extracted samples is given in Table 2. All the materials contain sulfur, and the sulfur

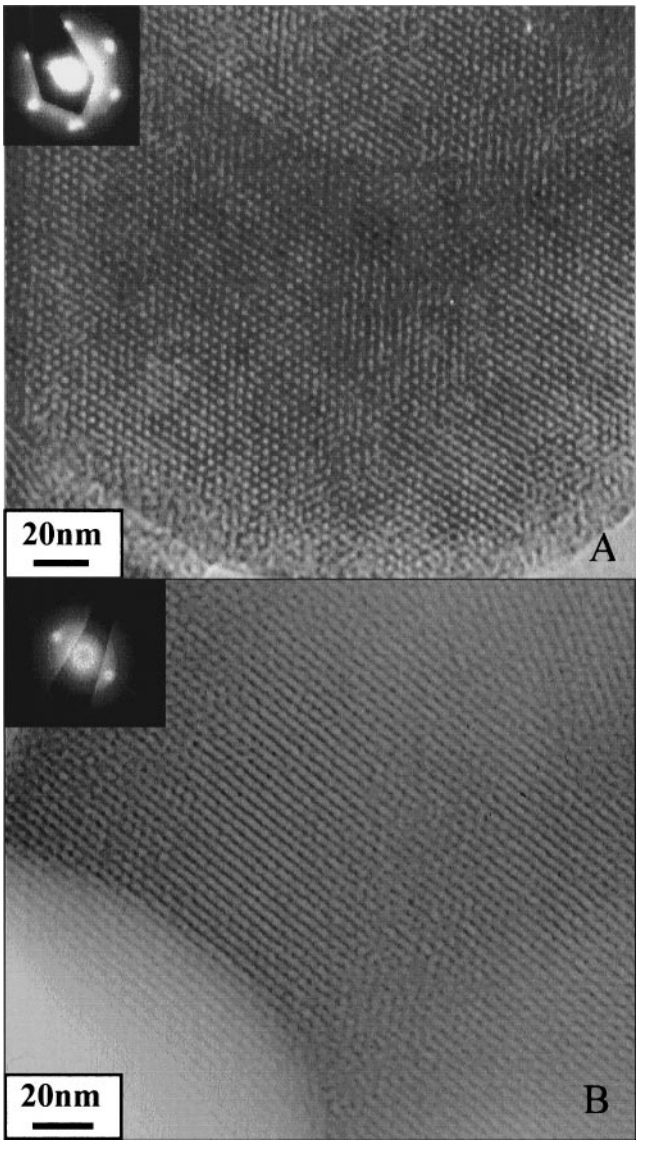

FIG. 2. TEM images of the M40 sample in a direction parallel (A) and normal (B) to the channel axis. Inset: selected area electron diffraction (ED) patterns.

content parallels the mercaptopropylsilane concentration in the synthesis mixture (Tables 1 and 2). Indeed, from the yield of solid product and the S content it can be estimated that the efficiency of MPTS incorporation into the MCM-41 matrix is better than 95% in all cases.

The C : S atomic ratio increases from 3.7 in the alkyl-free thiol–MCM-41 sample (M0e) to 4.5 for the propyl/thiol-MCM-41 (Mp10e) and 7.2 for the sample synthesized with the higher methylsilane concentration (M60e). This increase can be taken as an indication that these materials contain methyl (or propyl) beside mercaptopropyl groups. From the C and S content it would be possible to obtain the concentration of alkyl species, provided no other carbon-bearing chemical fragments were present in the solid. However, the C : S ratio of the sample prepared in the absence of alkylsilanes is 3.7, instead of the theoretical value of 3 for the Pr-SH fragment. This suggests that some unhydrolyzed methoxy groups of the alkoxy precursor still remain on the solid after template extraction. Therefore, the concentration of Me groups in the material cannot be deduced by simple calculation from the chemical analysis data. Nevertheless, the high C content of the sample obtained from methyl-rich synthesis mixture would be best explained by assuming that MTMS co-condenses with TMOS and MPTS.

The presence of methyl groups bonded to Si in the extracted samples is evidenced by the strong, sharp infrared band at 1276 cm^{-1} (Fig. 3), characteristic of the symmetric bending mode of the methyl group in methylsilanes (23–27). Also, a band at 2975 cm^{-1} is observed, the intensity of which increases with the nominal methyl content in the samples, that can be assigned to the asymmetric stretching mode of this group.

The concentration of surface methyl groups in the extracted samples has been estimated from the band at 1276 cm^{-1}, assuming that Beer's law is holding, as $C = A/\varepsilon$, where C is the concentration of $\equiv Si{-}CH_3$ species in moles per gram, A is the integrated absorbance of the band in centimeters per gram, and ε is the integrated absorptivity in centimeter per mole. The integrated absorptivity was estimated as 1.0 10^6 cm mol^{-1} from spectra of MTMS in solution, which showed the symmetric deformation band of the methyl group bonded to Si at 1267 cm^{-1}. The calculated Me : Si ratio in the extracted samples is reported in Table 2 and Fig. 4. The Me content of the solids closely corresponds to its molar fraction in the synthesis gel for low Me loading, and increases with the silane concentration (Fig. 4). However, the efficiency of the Me incorporation into the solid increases strongly at high Me loading.

Due to its low absorptivity, the S–H stretching band of propylthiol is observed, at ca. 2575 cm^{-1} (25), only in those samples with higher sulfur content. These species are better

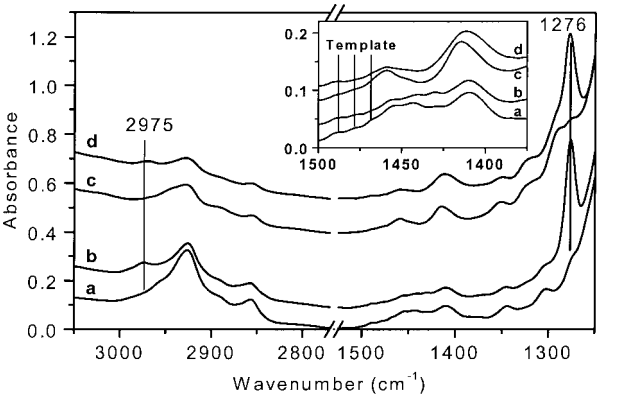

FIG. 3. FTIR spectra of (a) M10e, (b) M60e, (c) M10H, and (d) M60H samples. Spectra have been normalized according to the silica content in the sample and plotted offset for clarity.

TABLE 2

Chemical Composition and Surface Groups Density of Extracted [R/SH]–MCM-41 Materials and Their Oxidized Counterparts

Extr. sample	Elemental analysis (wt%) C	H	N	S	SiO_2[a] (wt%)	Me:Si	S:Si	Oxid. sample	SiO_2[a] (wt%)	S:Si	H^+:Si[b]
M0e	15.8	3.14	0.00	11.23	69.9	0	0.301				
M5e	17.3	3.34	0.27	9.92	69.6	0.014	0.267	M5H	63.4	0.210	0.131
M10e	16.7	3.51	0.19	9.65	69.8	0.028	0.259	M10H	60.4	0.222	0.143
M40e	14.0	3.03	0.23	6.73	74.3	0.15	0.170	M40H	68.2	0.155	0.078
M60e	12.1	2.58	0.17	4.60	80.2	0.33	0.108	M60H	77.8	0.107	0.042
Mp10e	16.0	3.21	0.15	9.56	71.6	0	0.250	Mp10H	62.3	0.233	0.120
Msil0[c]	5.9	1.70	0.13	1.70	85.7	0	0.037	Msil0H[d]	81.8	0.036	0.034

[a] Residual weight after TG calcination.
[b] Sulfonic acid content determined by titration.
[c] Sample prepared by sylilation with MPTS of a preformed MCM-41 material.
[d] Sample Msil0 oxidized with concentrated nitric acid.

identified by the methylene stretching bands of the propyl chain, in the region 2950–2850 cm^{-1}, and their deformation bands, at 1410, 1430, and 1455 cm^{-1} (Fig. 3). These bands can be assigned to the symmetric bending ("scissoring") mode of the three distinct methylene groups of the propyl chain. The first one, at 1410 cm^{-1}, is assigned to a methylene directly bonded to silicon (27) and is also present in the acidic samples. This band is broadened as it overlaps with the weak methyl asymmetric deformation band of the ≡Si–CH_3 species (24, 26, 27). The band at 1430 cm^{-1} would correspond to the methylene next to the thiol group (25, 27), while the band at 1455 cm^{-1} appears in the region of the methylene symmetric bending mode band in alkanes (23, 24, 27). Furthermore, a band that can be assigned to the methylene wagging mode in paraffinic chains (26, 27) appears at 1305 cm^{-1}.

The spectra of the extracted samples suggest that unhydrolyzed methoxy groups could also be present on the silica surface. Although the corresponding methyl stretching bands cannot be clearly observed due to the overlapping with the methylene stretching bands, absorption bands at ca. 1440 cm^{-1} can be identified that might be assigned to the methyl symmetric and asymmetric bending modes in methoxy species (23, 25).

The IR spectra show that traces of the template remain in the samples after the extraction (Fig. 3). Up to three weak bands can be identified at ca. 1490, 1480, and 1465 cm^{-1}. These are the three main bands in this region of the spectrum shown by the parent samples before extraction, and have been assigned to the asymmetric head group methyl (CH_3–N^+) bending mode (1490 and 1480 cm^{-1}) and the methylene symmetric bending mode (1465 cm^{-1}) of the cetyltrimethylammonium ion (28–30).

The FTIR spectra of the dry samples under vacuum do not show the characteristic hydroxyl stretching band at ca. 3750 cm^{-1} indicating that no free silanol species are present in these samples. However, a broad band ranging from 3700 to 3000 cm^{-1} is observed indicative of H-bonded internal hydroxyl species.

The reported results show that the co-condensation process of alkoxysilanes renders hybrid Me/SH materials with a high density of silane functional groups. From the S and Me content (Table 2), the molar ratio between functional groups and silicon atoms can be calculated. This ratio is 0.30 for the sample with no Me groups, remains practically constant up to the sample M40e, and rises to 0.44 for the material with the highest Me population (M60e). Therefore, in the last sample, on average 1 in 2.3 Si atoms is bearing an organic moiety. Such a high $Q_3/(Q_3 + Q_4)$ ratio is by no means uncommon in pure silica MCM-41 materials. For instance, a $Q_3/(Q_3 + Q_4)$ ratio of 0.44 is also reported in Ref. (13) for extracted HMS, used as substrate for mercaptopropylsilane anchoring.

The [Me/SH]–MCM-41 hybrid materials possess a surface area which is higher than that of the Me-free

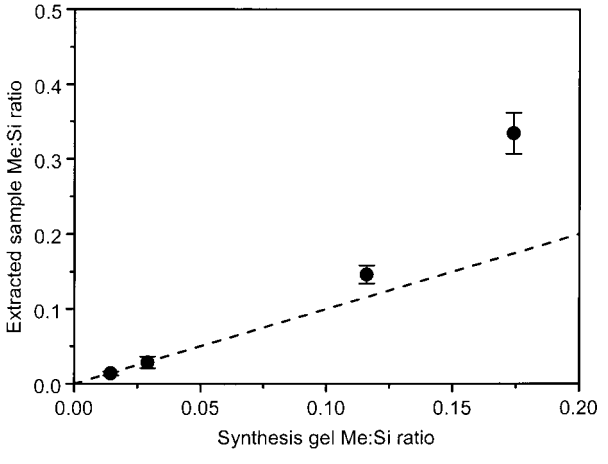

FIG. 4. Methyl groups content in extracted samples.

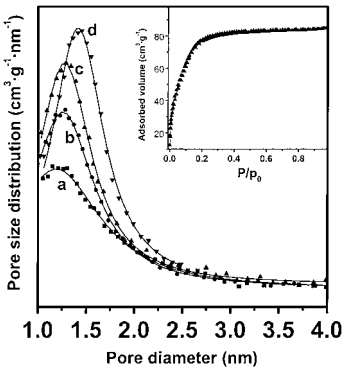

FIG. 5. BJH pore size distribution of (a) M0e, (b) M5e, (c) M40e, and (d) M60e extracted samples, from nitrogen adsorption/desorption isotherms at 77 K. Inset: nitrogen adsorption/desorption isotherm of sample M40e.

mercaptopropyl-containing sample (M0), and increases with the Me loading to reach a top value of ca. 850 $m^2 \cdot g^{-1}$ (Table 1). The pore size distribution obtained by N_2 adsorption is centered at a pore diameter of ca. 13 Å for all the samples (Fig. 5). However, it is well known (31–33) that, in general, the BJH method when applied to this region of pore size underestimates its value, as compared for instance with the value obtained from the Howarth–Kawazoe model by using Ar as adsorbate.

It is interesting that the pore size is not affected by the density of mercaptopropyl groups protruding from the silica surface into the channels nor by the presence of large amounts of Me groups. Indeed, the average pore diameter of the sample containing Pr instead of Me fragments is also 13 Å.

The as-made [Me/SH]–MCM-41 samples show two steps of weight loss, when heated under air flow, centered at 530 K (step I) and 640 K (step II), and a continuous weight loss (step III) from ca. 670 to 1100 K (Fig. 6). It is remarkable that practically no weight loss is observed up to 370 K, which indicates a nearly complete exclusion of water from the pores, proving the high hydrophobicity of these materials.

After treatment of the samples with the HCl/EtOH solution, step I disappears, being replaced by a small weight loss below ca. 350 K due to the desorption of water. In contrast, the organic material removed above 570 K (steps II and III) remains unaffected by the extraction procedure. This behavior allows us to assign the weight loss below 570 K to the decomposition of surfactant. In pure silica MCM-41, the decomposition of trimethylalkylammonium takes place at a similar temperature. The material desorbed at T higher than 570 K should therefore correspond in a major part to mercaptopropyl and in a lesser extent also to methyl groups.

The thermal decomposition of the surface species present in the extracted sample M60e under helium flow is also observed at temperatures above 570 K, and is accompanied by the detection of methanethiol and propanethiol in the

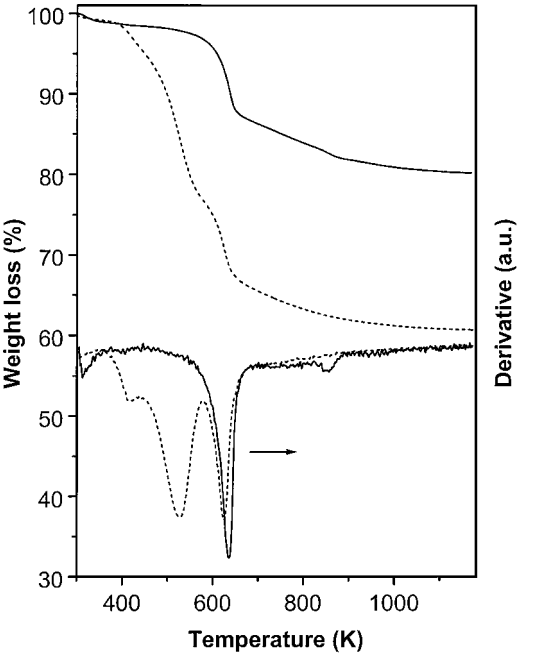

FIG. 6. TG/DTG curves of the as-made (dotted line) and extracted (full line) M60 sample under air flow.

gas phase, identified by MS at $m/z = 47$ and 76, respectively (Fig. 7).

It is remarkable that dimethyldisulfide (CH_3–S–S–CH_3) is detected among the gaseous products, at ca. 670 K, as

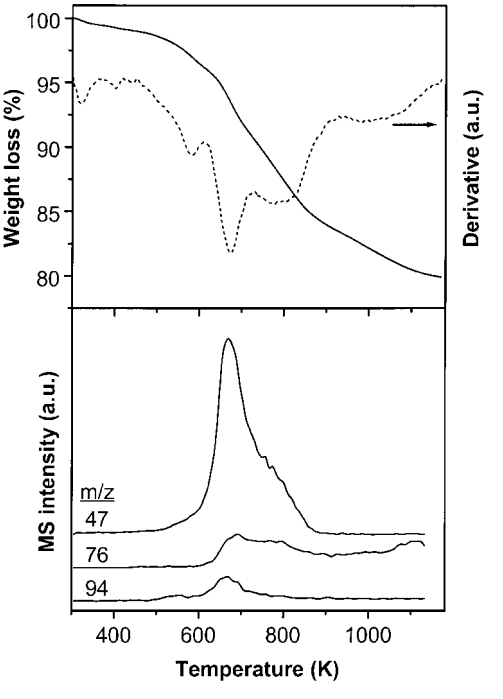

FIG. 7. TG/DTG curves of the extracted M60e sample under He flow, and MS analysis of the outlet gases. The MS signal intensity curves for selected m/z values are offset for clarity.

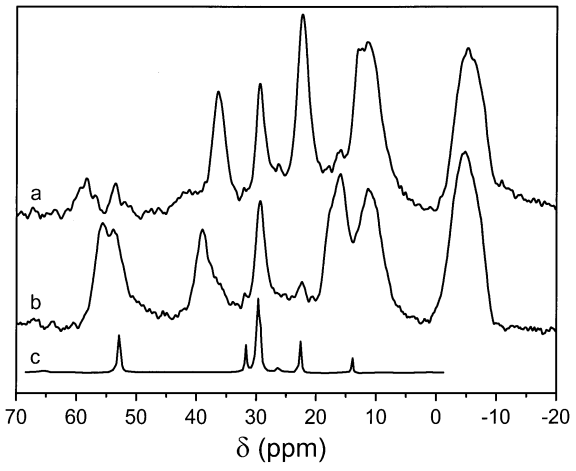

FIG. 8. ^{13}C CP/MAS NMR spectra of M60e (a) and M60H (b) samples. The spectrum (c) corresponds to a C_{16}TA-containing MCM-41 sample prepared as in Ref. (46).

revealed by the signal at $m/z = 94$ (Fig. 7). The simultaneous detection of a signal of similar intensity at $m/z = 74$ (not shown) supports this assignment and rules out the presence of 1,2-ethanedithiol. This result points to the possible existence of disulfide species on the extracted samples, although heat-promoted recombination of methylthiol in the gas phase could not be ruled out.

The ^{13}C CP MAS NMR spectrum of the extracted M60e sample is presented in Fig. 8. The proposed assignments for the observed resonance signals have been collected in Table 3. The chemical shifts for methyl and propylsulfur species present on the MCM-41 surface have been estimated according to the principle of additivity for the influence that a functional group in the vicinity of a given carbon atom has on its chemical shift (34, 35), and making use of reported chemical shifts for alkanes and alkylsulfur compounds (34, 36, 37) as well as alkyl and alkylthiol species anchored on silica and polysiloxanes (38–44). The assignment of carbon resonances in methoxy and ethoxy species is taken from the literature (39–42, 45).

TABLE 3

Assignment of the ^{13}C CP MAS NMR Spectra

Sample	δ (ppm)[a]	Atom[b]	Species
Me60e	−5	C^1	≡Si–CH_3
	29	C^2	≡Si–$(CH_2)_3$–SH
	22.4	C^3	≡Si–$(CH_2)_3$–SH
		C^2	≡Si–$(CH_2)_3$–S–S–$(CH_2)_3$–Si≡
	11–13	C^1	≡Si–$(CH_2)_3$–X[c]
	36.5	C^3	≡Si–$(CH_2)_3$–S–S–$(CH_2)_3$–Si≡
	52	C^1	≡Si–O–CH_3
	58.5	C^1	≡Si–O–CH_2–CH_3
	16	C^2	≡Si–O–CH_2–CH_3
Me60H	56	C^3	≡Si–$(CH_2)_3$–SO_3H
	18	C^2	≡Si–$(CH_2)_3$–SO_3H
	39	C^3	≡Si–$(CH_2)_3$–S–S(O)$_2$–$(CH_2)_3$–Si≡
	12	C^1	≡Si–$(CH_2)_3$–X[c]
	−5	C^1	≡Si–CH_3

[a] Chemical shift from TMS.
[b] Carbon atoms are numbered from the one closest to the Si atom.
[c] X stands for any sulfur-containing moiety.

The intense resonance signal centered at ca. −5 ppm corresponds to methyl groups bonded to Si. The peak at 29 ppm corresponds to the central methylene carbon (C^2 atom) of the propyl chain in the 3-mercaptopropyl moiety, while the carbon atom adjacent to the SH moiety (C^3) produces a peak at 22.4 ppm. Although these two resonances would be expected to overlap, Feng *et al.* (12) reported such an assignment in samples with a high loading of mercaptopropyl species. These authors attributed the observed splitting to a conformational effect due to the close packing of the propyl chains. As for the carbon atom bonded to silicon (C^1), it is expected to contribute to the broad signal centered at ca. 12 ppm.

In addition, several resonances are observed that cannot be assigned to methyl or propylthiol species. An intense peak can be distinguished at 36.5 ppm, which could be assigned to the C^3 atom adjacent to S atoms in dipropyldisulfide species. The C^1 resonance of this species would appear close to the C^1 of 3-mercaptopropyl, contributing in this way to the broad signal observed at ca. 12 ppm, whereas the central methylene group (C^2) of the propyl chain of disulfides would resonate at ca. 22.4 ppm, overlapping with the C^3 of propylthiol. Also, two weak resonances appear at 52 and 58.5 ppm. The first one may arise probably from unhydrolyzed methoxy groups, whereas that at lower field could correspond to the methylene in ethoxy groups, which could be present in the solid as a result of alkoxy exchange between the methoxy fragments present in the solid and the ethanol used as solvent during the extraction procedure. According to the spectrum of a MCM-41 sample containing C_{16}TA (Fig. 8), prepared as in Ref. (46), other weaker resonances detected in the spectrum of the M60e sample could arise from the residual amount of C_{16}TA/C_{12}TA still present in the extracted (and oxidized) materials, as observed by IR spectroscopy.

It is interesting to notice that the ^{13}C CP MAS NMR reveals several features, such as the splitting of C^3 and C^2 signals of 3-mercaptopropylthiol and the prominent presence of disulfide, which are characteristics of materials with a high S loading. However, the sample M60e has a sulfur content of only 1.4 mequiv g^{-1}. Therefore, these results suggest that the propylthiol chains are closer than what would be anticipated from a full random distribution over the silica surface.

The external surface of the samples has been characterized by XPS. Figure 9 shows the S 2*p* core-level spectra of two [R/SH]–MCM-41 extracted samples, with low (M10e) and high (M60e) methyl content. The spectrum of an

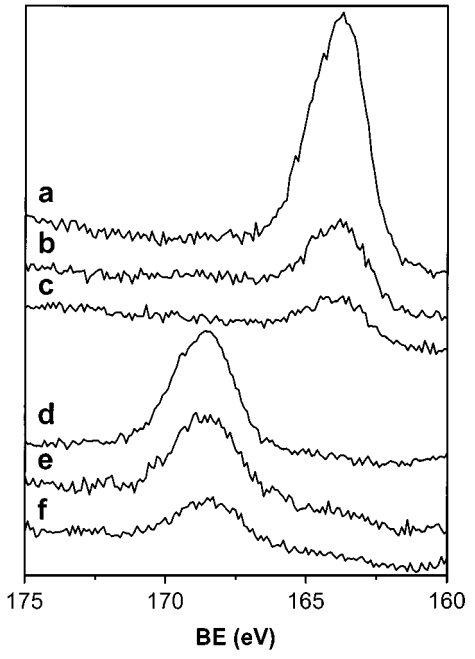

FIG. 9. S 2*p* core-level spectra of (a) M10e, (b) M60e, (c) Msil0, (d) M10H, (e) M60H, and (f) Msil0H.

[SH]–MCM-41 sample (Msil0), prepared by silylation with MPTS of a preformed MCM-41 material, is also reported in Fig. 9.

Owing to the synthesis procedure and the low sulfur content of the Msil0 sample (Table 2), propylthiol is the only sulfur species expected to be present in this sample. Indeed, the XPS spectrum of the Msil0 sample shows a single S 2*p* peak at 163.7 eV, which is within the range of binding energy of thiol species (47). Both M10e and M60e spectra also show a single S 2*p* peak at 163.7 eV indicative of the presence of thiol. However, disulfide species have an S 2*p* binding energy which is higher than that of thiol by less than 1 eV (47). Therefore, the presence of disulfide species in these samples cannot be excluded as the corresponding S 2*p* peak would overlap with the thiol peak.

The S : Si ratios calculated for these samples from the XPS spectra (Table 4) are only slightly higher than the average S : Si ratios (Table 2). This result shows that the sulfur species are in fact dispersed within the porous structure of the material.

TABLE 4

External Surface S : Si Ratio As Determined by XPS

Extracted sample	S : Si	Oxidized sample	S : Si
M10e	0.360	M10H	0.215
M60e	0.112	M60H	0.091
Msil0	0.042	Msil0H	0.060

(b) Pore Size Modification

The esterification reaction of glycerol with fatty acids, which involves bulky molecules, could be controlled by the pore size of the MCM-41 catalyst. For this reason, several modifications of the base synthesis gel composition for an SH/Me ratio of 9 have been introduced in order to control the pore size of the hybrid material.

In one example (Ms10, Table 1) the C_{16}/C_{12} mixture of trimethylalkylammonium cation was replaced by C_{12}/C_{10}. An MCM-41 material with a single d_{100} XRD reflection is obtained, from which a unit cell size of 33.5 Å was estimated, smaller than that of the standard preparation, in both the as-made and extracted materials. This can be attributed to the shortening of the hydrocarbon tail of the surfactant. The BET surface area was 745 $m^2\ g^{-1}$ and the pore volume decreased to 0.18 ml g^{-1}. The average pore size is below 10 Å, beyond the limit of applicability of the BJH method for the N_2 isotherm. From the unit cell reduction as compared with the standard material containing C_{16}/C_{12}, the pore size can be estimated to be 6–7 Å smaller in this material.

TMB was selected as swelling agent, with the aim of increasing the pore size of the MCM-41 materials. However, the addition of TMB (TMB/surfactant = 0.5 and 1.0) to the synthesis gel used to prepare the M10 sample (Table 1) resulted in a less organized material, as evidenced by a broadening of the XRD pattern. Furthermore, although an improved ordering (according to XRD) was obtained by decreasing the surfactant/SiO_2 ratio to 0.08 (TMB/surfactant = 1), the resulting material showed no increase in the pore size with respect to the M10e sample, which indicates that the Me/SH sample does not swell in the presence of TMB under the conditions described above. Indeed, no TMB was detected by mass spectrometry in the gases released from the as-made sample during heating under helium flow.

(c) Oxidized Samples

The transformation of the thiol groups of MCM-41 materials into sulfonic acid, the active center in acid-catalyzed reactions, is carried out by oxidation. Several oxidation procedures have been described in the literature. Lim *et al.* (15) reported the use of nitric acid, whereas Van Rhijn *et al.* (16) preferred hydrogen peroxide for this purpose. We have found before that the oxidation with nitric acid of SH–MCM-41 synthesized by co-condensation leads to a catalyst with a high content of disulfide groups on its surface (48). Therefore, the [Me/SH]–MCM-41 samples were oxidized with hydrogen peroxide, according to the procedure outlined in the experimental section. However, as will be described in this section, this procedure did not result in the complete oxidation of sulfur into sulfonic acid.

The sulfur content of the oxidized samples is slightly lower than that of their extracted counterparts (Tables 2

and 4). However, the fraction of sulfur removed during oxidation decreases with the thiol content. Thus, 100% of S retention is found for the sample with the lowest thiol content (M60e).

After the oxidation treatment, the materials seem to retain a high ordering as no change in the XRD patterns is observed (Fig. 1).

It is interesting that the number of Brønsted acid sites is lower than that of sulfur atoms (Table 2), and that the H^+ : S ratio decreases as the samples become richer in Me and poorer in S. Indeed, an exchange capacity of 1.76 mequiv g^{-1} is reported in Ref. (15) for a sulfonic acid–MCM-41 sample obtained by co-condensation and subsequent oxidation, which is reported to contain 4.7 mequiv of S per g of SiO_2 in the extracted product. In our case, the deviation of the H^+ : S ratio from 1 cannot be attributed to an eventual loss of S during oxidation, but can be attributed to an incomplete oxidation of the sulfur-bearing species present in the extracted material.

The chemical nature of the organic species present in the oxidized material can be conveniently studied by NMR. The ^{13}C CP MAS NMR spectrum of the M60H sample shows several resonance signals (Fig. 8) that correspond to a variety of organosulfur species. The signal corresponding to the carbon adjacent to the S atom (C^3) in PrSH (22.4 ppm) disappears by oxidation. New intense signals develop at 18 ppm and 56 ppm which are assigned to C^2 and C^3, respectively, in propylsulfonic groups (Table 3). The peak at 36.5 ppm assigned to disulfide species in the extracted material is shifted high field to 39 ppm after oxidation. This signal could tentatively be assigned to the carbon atom next to the S atom of thiosulfonate species, R–S(O)$_2$–S–R. Van Rhijn *et al.* (16) reported a broad resonance line at 41 ppm in oxidized S-bearing MCM-41 materials prepared by surface coating. Although the authors assigned this signal to dipropyldisulfide species, our estimation of chemical shifts suggests that it would rather correspond to a more oxidized sulfur species. Finally, the intense peak at ca. −5 ppm indicates that the Me groups are still present in the oxidized materials.

The quantitative retention of Me groups after oxidation is also deduced from the intense IR band at 1276 cm^{-1} (Fig. 3). The methylene wagging band that appears at 1305 cm^{-1} in the extracted sample shifts to 1290 cm^{-1} after oxidation, and appears as a shoulder of the 1276 cm^{-1} band characteristic of the methyl group bonded to silicon. This makes less accurate the estimation of the Me : Si ratio, from the 1276 cm^{-1} band intensity as it was done for the extracted samples. However, the intensity of the 1276 cm^{-1} band, in the spectra normalized respect to the silica content of the sample, seems not to be significantly modified after oxidation. For this reason, we estimate the Me : Si ratio in the acidic samples to be the same as that in the extracted counterparts.

Upon oxidation, new IR bands develop at 1350 and 1325 cm^{-1} that are in the region for the asymmetric stretching band of SO_2 moieties (23–25, 27, 49), thus supporting the proposed formation of sulfonic acid species.

Finally, the IR spectra of the acidic samples do not show bands at ca. 1440 cm^{-1}, previously assigned to methoxy species, which would have been removed during oxidation.

According to these results, the low H^+ : S ratio found in the oxidized materials could be attributed to the stability of the S–S bridge already present in the extracted sample under the chemical environment prevalent in the oxidation process, rather than being due to a partial oxidation of SH groups. The formation of disulfide species could take place during the synthesis of the parent gels, as this condensation of thiol groups has already been reported to occur in alkaline aqueous solution (50). In order to reach quantitative yield in the oxidation of sulfur to sulfonic acid, the presence of such stable disulfide species in the extracted material should first be avoided.

The S 2*p* core-level peak of the oxidized M10H and M60H samples, as well as the reference sample Msi10H, is shifted ca. 5 eV to higher binding energy, with respect to their propylthiol-bearing precursors (Fig. 9), evidencing a high oxidation state of the sulfur species (47). Indeed, all the sulfur species in the Msi10H sample are present as sulfonic acid, as indicated by its H^+ : S ratio close to 1 (Table 2). These results tend to support the hypothesis that the sulfur species present in the hybrid methyl/sulfonic acid materials are in a high oxidation state, while thiol or disulfide species are not observed in the XPS spectra of these oxidized materials.

During heating under an air flow, the oxidized samples exhibit a first weight loss step below 370 K (Fig. 10) that corresponds to the desorption of water. Two further steps of weight loss can be clearly distinguished, centered at ca. 590 K and 720 K, that should correspond to the decomposition/combustion of organic fragments and sulfur-bearing species. For the sample with the highest Me loading (M60H), an additional weight loss is detected at 820 K, which is also observed at the same temperature in a reference sample containing Me groups only (not shown). Therefore, this thermal feature could be attributed to the release of Me groups attached to Si. Furthermore, an additional peak at ca. 530 K can be distinguished in the DTG curve of this sample.

Under a helium flow, the decomposition products start to be detected in the gas phase from 470 K (Fig. 11). Above 570 K, SO_2 is the main product detected and the rate of weight loss parallels that of SO_2 production, showing a maximum at ca. 760 K. At lower temperatures, small amounts of SO_2, dimethyldisulfide ($m/z = 94$), and methanethiol ($m/z = 47$) are observed, the last compound being probably the result of the cracking of disulfide species.

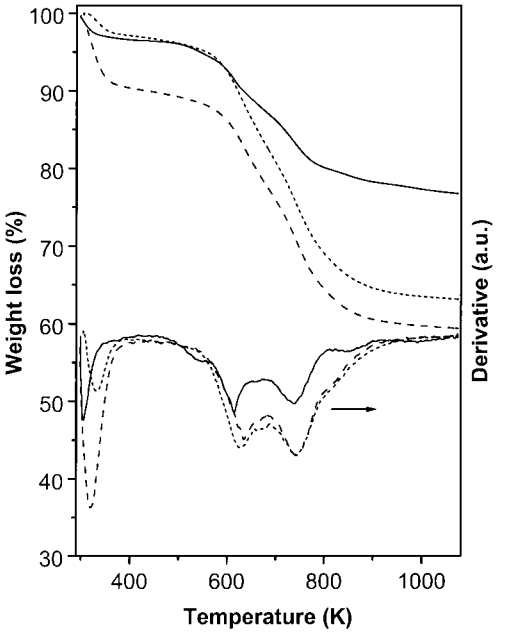

FIG. 10. TG/DTG curves of M5H (dotted line), M10H (dashed line), and M60H (full line) samples under air flow.

The rate of weight loss strongly increases with the temperature as it approaches ca. 470 K (Fig. 10). Therefore, this could be taken as a practical upper temperature limit for using the [Me/SO_3H]–MCM-41 materials in catalytic processes in order to avoid unaffordable loss of sulfur. However, it will be shown in part 2 of this work (20) that during the batch esterification of glycerol with fatty acids some sulfur is lost at a temperature as low as 393 K, and this loss increases to a great extent at 423 K.

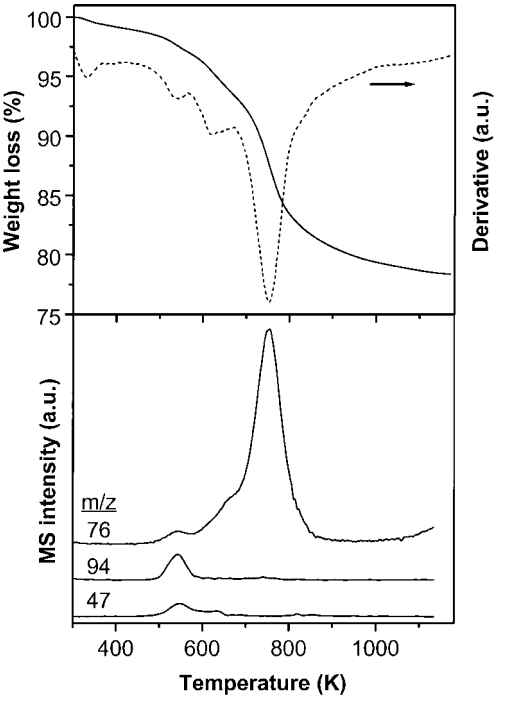

FIG. 11. TG/DTG curves of the oxidized M60H sample under He flow, and MS analysis of the outlet gases. The MS signal intensity curves for selected m/z values are offset for clarity.

DISCUSSION

The information supplied by the different characterization techniques on the nature and concentration of the several organic species covering the walls of the MCM-41 channels, together with the surface area data, could be combined to build up a simple model on the arrangement of the organic fragments on the pore surface.

The average density of functional groups, estimated from the surface area and the total silane content, is close to 3 organic moieties per 100 $Å^2$ for most of the [R/SH]–MCM-41 samples, and ca. 4 for the sample with the highest Me content. Then, the average distance between organic groups can be estimated to be in the range 5–6 Å. It is interesting that the average Si-to-Si distance in silicas and silicates is 3.06 Å (51), i.e., nearly half the R···R distance (R = Me or PrSH species) estimated in the functionalized materials. Thus, a model of hybrid MCM-41 materials in which, on average, the silicon [O_3RSi] species alternate with those having four oxygen atoms in the first coordination shell, [SiO_4], would be consistent with the experimental data.

The average distance between mercaptopropyl moieties can also be calculated following this random model. This average, statistical distance increases smoothly from ca. 5 Å for the Me-free sample, to ca. 10 Å for the highest Me loading (M60). A 5-Å separation would eventually make plausible the formation of S–S bonds (which average bond length is 2.1 Å), but it would be less probable as the average distance increases. Nonetheless, a large fraction of disulfide bridges are still present in sample M60. Indeed, in the oxidized samples, the H^+/S ratio decreases as the Me content increases; i.e., the probability of disulfide bridge formation parallels the incorporation of methyl moieties. This behavior, opposite to what would be expected from increasing the "dilution" of the S species all over the MCM-41 surface, would suggest that the progressive incorporation of Me groups produces a nonrandom distribution of S-containing groups, which seem to cluster upon the surface. On a molecular scale, there would be alkyl-S regions separated by Me areas, as has been represented in Fig. 12.

The cross sections of a propyl chain and a methyl group can be estimated as 4.5 and 4 Å, respectively (52). Taking into account the average R···R distance estimated before, these values correspond to a nearly close packing of organic groups lining the channel wall. A full covering of the MCM-41 surface by organic groups could have important consequences for the catalytic activity of the oxidized materials. The polar oxygen atoms of the silica framework and

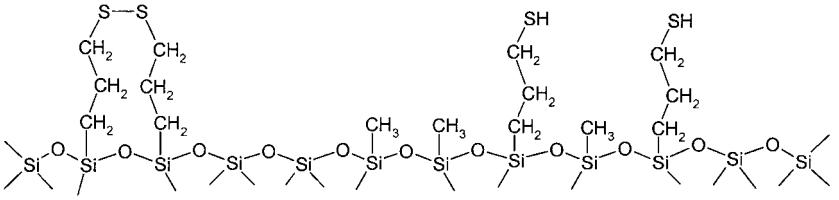

FIG. 12. Schematic representation of the surface of the [Me/SH]–MCM-41 materials.

the bridge silanol groups still present in the material are both hindered by the tight arrangement of organic groups, in such a way that from the highly hydrophobic Me (or Pr)-covered surface strongly polar sulfonic groups emerge. The relevance of this surface of modulated polarity on the catalyst activity and selectivity in the esterification reaction of glycerol with fatty acids will be described in part 2 of this work (20).

CONCLUSIONS

Well-ordered MCM-41 materials bearing alkyl (methyl and propyl) and mercaptopropyl groups have been prepared by one-step hydrothermal synthesis. Moreover, it has been possible to obtain these materials in a broad range of methyl/mercaptopropyl ratios.

The average pore size can be conveniently tuned by changing the alkyl chain length of the trimethylalkylammonium surfactants, whereas the use of trimethylbenzene as a potential swelling agent has no effect on the pore size.

The organic functional groups which line the channels wall are arranged in a nearly close-packed configuration.

After oxidation of the materials with hydrogen peroxide, the pore ordering as well as the methyl groups and most of the S-bearing species were preserved. Indeed, sulfonic acid groups and chemical species resulting from partial oxidation of sulfur are detected in the solid after the oxidation treatment.

ACKNOWLEDGMENTS

The authors acknowledge the C.A.M. (Spain), Project 06M/084/96, and CICYT (Spain), Project MAT97-1207-C03-02, for financial support. I.D. acknowledges the Spanish Ministry of Education for a Ph.D. grant. The authors thank Dr. T. Blasco for collecting the ^{13}C NMR MAS spectra and Prof. J. L. G. Fierro for collecting the XPS spectra.

REFERENCES

1. Lauridsen, J. B., *J. Am. Oil Chem. Soc.* **53**, 400 (1976).
2. Jungermann, E., *Cosmet. Sci. Technol. Serv.* **11**, 97 (1991).
3. Corma, A., Iborra, S., Miquel, S., and Primo, J., *J. Catal.* **173**, 315 (1998).
4. Sonntag, N. O. V., *J. Am. Oil Chem. Soc.* **59**, 795A (1982).
5. Devinat, G., and Coustille, J. L., *Rev. Fran. Corps Gras* **30**, 463 (1983).
6. Corma, A., García, H., Iborra, S., and Primo, J., *J. Catal.* **120**, 78 (1989).
7. Heykants, E., Verrelst, W. H., Parton, R. F., and Jacobs, P. A., *Stud. Surf. Sci. Catal.* **105**, 1277 (1996).
8. Machado, M. d. S., Cardoso, D., Sastre, E., and Pérez-Pariente, J., *Appl. Catal.*, in press.
9. Abro, S., Pouilloux, Y., and Barrault, J., *Stud. Surf. Sci. Catal.* **108**, 539 (1997).
10. Díaz, I., Martínez-Guereñu, A., Mohino, F., Pérez-Pariente, J., and Sastre, E., Proceedings of the XVII Iberoamerican Catalysis Symposium, Porto, July, 2000.
11. Bossaert, W. D., De Vos, D. E., Van Rhijn, W. M., Bullen, J., Grobet, P. J., and Jacobs, P. A., *J. Catal.* **182**, 156 (1999).
12. Feng, X., Fryxell, G. E., Wang, L. Q., Kim, A. Y., Liu, J., and Kemner, K. M., *Science* **276**, 923 (1997).
13. Mercier, L., and Pinnavaia, T. J., *Adv. Mater.* **9**, 500 (1997).
14. Van Rhijn, W. M., De Vos, D. E., Sels, B. F., Bossaert, W. D., and Jacobs, P. A., *Chem. Commun.* 317 (1998).
15. Lim, M. H., Blanford, C. F., and Stein, A., *Chem. Mater.* **10**, 467 (1998).
16. Van Rhijn, W. M., De Vos, D., Bossaert, W., Bullen, J., Wouters, B., Grobet, P. J., and Jacobs, P. A., *Stud. Surf. Sci. Catal.* **117**, 183 (1998).
17. Koya, M., and Nakajima, H., *Stud. Surf. Sci. Catal.* **117**, 243 (1998).
18. Tatsumi, T., Koyano, A., and Igarashi, N., *Chem. Commun.* 325 (1998).
19. Corma, A., Domine, M., Gaona, J. A., Jorda, J. L., Navarro, M. T., Rey, F., Pérez-Pariente, J., Tsuji, J., McCulloch, B. M., and Nemeth, L. T., *Chem. Commun.* 2211 (1998).
20. Díaz, I., Márquez-Alvarez, C., Mohino, F., Pérez-Pariente, J., and Sastre, E., *J. Catal.* **193**, 295 (2000).
21. Díaz, I., Pérez-Pariente, J., and Sastre, E., Proceedings of the Spanish Catalysis Society-SECAT99, Cádiz, September, 1999.
22. Díaz, I., Mohino, F., Pérez-Pariente, J., and Sastre, E., *Appl. Catal.*, in press.
23. Smith, B., "Infrared Spectral Interpretation. A Systematic Approach." CRC Press, Boca Raton, 1999.
24. Bellamy, L. J., "The Infrared Spectra of Complex Molecules." Chapman and Hall, London, 1975.
25. Roeges, N. P. G., "A Guide to the Complete Interpretation of Infrared Spectra of Organic Structures." Wiley, Chichester, 1994.
26. Szymanski, H. A., "Interpreted Infrared Spectra." Plenum, New York, 1964.
27. Colthup, N. B., Daly, L. H., and Wiberly, S. E., "Introduction to Infrared and Raman Spectroscopy." Academic Press, Boston, 1990.
28. Calabro, D. C., Valyocsik, E. W., and Ryan, F. X., *Microporous Mater.* **7**, 243 (1996).
29. Wong, T. C., Wong, N. B., and Tanner, P. A., *J. Colloid Interface Sci.* **186**, 325 (1997).
30. Holmes, S. M., Zholobenko, V. L., Thursfield, A., Plaisted, R. J., Cundy, C. S., and Dwyer, J., *J. Chem. Soc., Faraday Trans.* **94**, 2025 (1998).
31. Kruk, M., Jaroniec, M., and Sayari, A., *Langmuir* **13**, 6267 (1997).
32. Lastoskie, C., Gubbins, K. E., and Quirke, N., *J. Phys. Chem.* **97**, 4786 (1993).
33. Ravikovitch, P. I., Odomhnaill, S. C., Neimark, A. V., Schuth, F., and Unger, K. K., *Langmuir* **11**, 4765 (1995).
34. Pretsch, E., Clerc, J. T., Seibl, J., and Simon, W., "Tables of Spectral Data for Structure Elucidation of Organic Compounds." Springer, Berlin, 1989.

35. Fürs, A., and Pretsch, E., *Anal. Chim. Acta* **229**, 17 (1990).
36. King, J. F., *in* "The Chemistry of Sulphonic Acids, Esters and Their Derivatives" (S. Patai and Z. Rappoport, Eds.), p. 249. Wiley, Chichester, 1991.
37. Fujihara, H., and Furukawa, N., *in* "The Chemistry of Sulphinic Acids, Esters and Their Derivatives" (S. Patai, Ed.), p. 275. Wiley, Chichester, 1990.
38. Hays, G. R., Clague, A. D. H., and Huis, R., *Appl. Surf. Sci.* **10**, 247 (1982).
39. Bayer, E., Albert, K., Reiners, J., Nieder, M., and Müller, D., *J. Chromatogr.* **264**, 197 (1983).
40. El-Nahhal, I. M., Yang, J. J., Chuang, I.-S., and Maciel, G. E., *J. Non-Cryst. Solids* **208**, 105 (1996).
41. Yang, J. J., El-Nahhal, I. M., and Maciel, G. E., *J. Non-Cryst. Solids* **204**, 105 (1996).
42. Maciel, G. E., Sindorf, D. W., and Bartuska, V. J., *J. Chromatogr.* **205**, 438 (1981).
43. Zaper, A. M., and Koenig, J. L., *Polym. Compos.* **6**, 156 (1985).
44. Leyden, D. E., Kendall, D. S., and Waddell, T. G., *Anal. Chim. Acta* **126**, 207 (1981).
45. de Haan, J. W., van den Bogaert, H. M., Ponjeé, J. J., and van de Ven, L. J. M., *J. Colloid Interface Sci.* **110**, 591 (1986).
46. Kolodziejski, W., Corma, A., Navarro, M. T., and Pérez-Pariente, J., *Solid State NMR* **2**, 253 (1993).
47. Wagner, C. D., Riggs, W. M., Davis, L. E., Moulder, J. F., and Muilenberg, G. E., "Handbook of X-Ray Photoelectron Spectroscopy." Perkin-Elmer, Eden Prairie, MN, 1979.
48. Mohino, F., Díaz, I., Pérez-Pariente, J., and Sastre, E., Proceedings of the Spanish Catalysis Society-SECAT99, Cádiz, September, 1999.
49. Bellamy, L. J., "Advances in Infrared Group Frequencies." Chapman and Hall, London, 1968.
50. Mohino, F., M.Sc. Thesis, Universidad Complutense de Madrid, 1988.
51. O'Keaffe, M., and Hyde, B. G., *in* "Structure and Bonding in Crystals" (M. O'Keaffe and A. Navrotsky, Eds.), Vol. I, p. 227. Academic Press, New York, 1981.
52. Breck, D. W., "Zeolite Molecular Sieves." Wiley, New York, 1974.